Angewandte Chemie
Eine Zeitschrift der Gesellschaft Deutscher Chemiker

Supporting Information

Metal-Insulator-Semiconductor Anodes for Ultrastable and Site-Selective Upconversion Photoinduced Electrochemiluminescence

Y. Zhao, J. Descamps, S. Ababou-Girard, J.-F. Bergamini, L. Santinacci, Y. Léger, N. Sojic*, G. Loget**

Metal-Insulator-Semiconductor Anodes for Ultrastable and Site-Selective Upconversion Photoinduced Electrochemiluminescence

Yiran Zhao,[a] Julie Descamps,[b] Soraya Ababou-Girard,[c] Jean-François Bergamini,[a] Lionel Santinacci,[d] Yoan Léger,*[e] Neso Sojic,*[b] Gabriel Loget*[a]

a. Univ Rennes, CNRS, ISCR (Institut des Sciences Chimiques de Rennes)-UMR6226, Rennes F-35000, France.
gabriel.loget@univ-rennes1.fr

b. University of Bordeaux, Bordeaux INP, ISM, UMR CNRS 5255, Pessac 33607, France.
neso.sojic@enscbp.fr

c. Univ Rennes, CNRS, IPR (Institut de Physique de Rennes)-UMR 6251, F-35000 Rennes, France.

d. Aix-Marseille Univ, CNRS, CINaM, Marseille, France.

e. Univ Rennes, INSA Rennes, CNRS, Institut FOTON-UMR 6082, F-35000, Rennes, France.
yoan.Leger@insa-rennes.fr

Table of contents

1. Methods

Reagents

Acetone (MOS electronic grade, Erbatron from Carlo Erba) and anhydrous ethanol (RSE electronic grade, Erbatron from Carlo Erba) were used without further purification. The ultrapure water had a resistivity of 18.2 MΩ cm (Purelab Classic UV). Sulfuric acid (96%, VLSI grade Selectipur) and hydrogen peroxide (30%, VLSI, Sigma-Aldrich) were purchased from BASF and Sigma Aldrich, respectively. Tris(bipyridine)ruthenium(II) chloride hexahydrate ($Ru(bpy)_3Cl_2 \cdot 6H_2O$, powder) and tri-n-tripropylamine (TPrA, ≥98%) were purchased from Sigma Aldrich. Phosphate buffer solution (PBS, 100 mM, pH 7.3) was prepared from potassium phosphate dibasic ((≥98%, ACS reagent) and sodium phosphate monobasic monohydrate (≥99.0%, ReagentPlus®) that were purchased from Sigma Aldrich.

Surface preparation and characterization

All vials and tweezers used for cleaning silicon were previously decontaminated in 3/1 v/v concentrated H_2SO_4/30% H_2O_2 at 105 °C for 30 min, followed by copious rinsing with ultrapure water. *Caution: the concentrated aqueous H_2SO_4/H_2O_2 (piranha) solution is very dangerous, particularly in contact with organic materials, and should be handled extremely carefully.* The *n*-type silicon wafers (0.3-0.7 Ω cm resistivity, phosphorus-doped, single side polished, 475-525 µm) (100) and the p^{++}-type silicon wafers (0.001-0.005 Ω cm resistivity, boron-doped, single side polished, 490-510 µm) (100) were purchased from University Wafers. All the Si surfaces were degreased by sonication in acetone, ethanol, and ultrapure water for 10 min respectively. The Si surfaces were then decontaminated and oxidized in piranha solution at 105 °C for 30 min, followed by rinsing with copious amounts of ultrapure water and dried under Ar flow. The metal thin films (Pt, Ir, Ru) were deposited on the clean *n*-Si/SiO_x surfaces by sputtering with a Leica EM ACE600 coating system (Pt target purity: 99.99%, Leica; Ir target purity: 99.95%, Neyco; Ru target purity: 99.9%, Neyco). The thickness of the film was controlled *in-situ* using a quartz crystal microbalance (QCM) and determined *ex-situ* by atomic force microscopy (AFM), as follows. Thickness calibration for each metal was done using a photoresist lift-off process to find out the relationship between the QCM value and the real value determined by AFM. Scanning electron

microscopy (SEM) was performed on a JSM 7100F (JEOL). XPS measurements were performed with an Mg K_{alpha} (hv = 1254.6 eV) X-ray source using a VSW HA100 photoelectron spectrometer with a hemispherical photoelectron analyzer, working at an energy pass of 20 eV. The experimental resolution was 1.0 eV. C 1s set at 284.8 eV was used as the energy reference for all the analyses. AFM images were acquired on a NT-MDT Ntegra microscope in semi-contact mode with FM tips (APPNANO, SPM Probe Model: FORTA-50, resonance frequency: 43-81 kHz). The images were treated and analyzed with the open-source Gwyddion software.

Electrochemical experiments

The coated surfaces Si surfaces (1.5 x 1.5 cm^2) were processed to fabricate the electrodes. An Ohmic contact was done on the backside of Si wafer by scratching the surface with a diamond glass cutter; then a droplet of InGa eutectic (Sigma Aldrich, 99.99%, metals basis) and a copper tape was applied on the scratched part. A thin layer of silver paste (Electron Microscopy Sciences) was painted to cover the InGa eutectic contact as well as a part of the copper tape. After the drying of the paste, Kapton tape was deposited to shield the backside for the protection of ohmic contact. Before their use in electrochemical experiments, the unmodified hydrogenated Si electrode (p^{++}-Si-H) was dipped for 1 min in 10% HF. The electrochemically active electrode surface is 0.5 cm^2, as determined by the O-ring of the cell. All (dark and illuminated) electrochemical experiments (CVs and CPs) were performed in the cell shown in Figure S11 that was mounted on the optical setup that is presented in Figure S12. The homemade cell was manufactured by a 3D printer in a Teflon piece and the optical window was a glass square. The PECL cell was designed with the Tinkercad application (https://www.tinkercad.com/). It was processed in PTFE on a ZMorph VX 3D printer equipped with CNC milling tool. Two holes (not shown in Figure S11) were drilled on both sides of the cell to allow the renewal of the electrolyte. The optical setup is composed of an 805 nm-dichroic mirror allowing to homogeneously illuminate the working electrode with the 850 nm spot (cleaned by an 850 ±10 nm band-pass filter) generated by the IR LED (the power density of the LED is 20 mW cm^{-2}). The emitted light is transmitted through the dichroic mirror, filtered by a 750 nm low-pass filter, and was measured by a spectrometer coupled to

an optical fiber. Two similar PECL setups coupled with two different spectrometers and potentiostats were set, one at ISCR (Rennes) that was coupled with an FLMT04304 Ocean Optics spectrometer and an SP300 (Biologic) potentiostat and one at ISM (Bordeaux) that was coupled with a Spectra pro 2300i (Princeton Instrument) spectrometer and a µAutolab Type II (Autolab) potentiostat. Both PECL setups gave similar results. The reference electrode was an Ag/AgCl (3 M KCl) electrode. The auxiliary electrode was a carbon rod. The working electrodes were the Si-based anodes. The electrolyte comprised 5 mM $[Ru(bpy)_3]^{2+}$, 0.1 M TPrA in PBS with a pH adjusted to 7.4. This composition of the solution is classically used for bioassays because it provides strong ECL intensity (see ref. 24 in the main manuscript). The electrochemical experiments were performed in air-equilibrated solutions. ECL spectrum was recorded by a spectrometer connected to an optical fiber. The cell was connected to a peristaltic pump (Yanmis) allowing the electrolyte to flow from bottom to top at a flow rate of 0.7 ml s^{-1} when CP was recorded. The hyperspectral confocal apparatus consists of an x4 magnification homemade microscope which images the electrode plane (the PECL spot) onto the slits of an IHR320 Horiba spectrometer with a Horiba Sincerity open electrode Si CCD camera. The spectrometer can be both used at zeroth order with opened entrance slits for direct imaging onto the CCD or at the first order with 50 µm slits for hyperspectral imaging. In the latter case, the spectral information is recorded for each position in the image along the slits of the spectrometer. This allows extracting spectrally-filtered images of the laser spot and PECL spots along one direction.

2. Supplementary figures

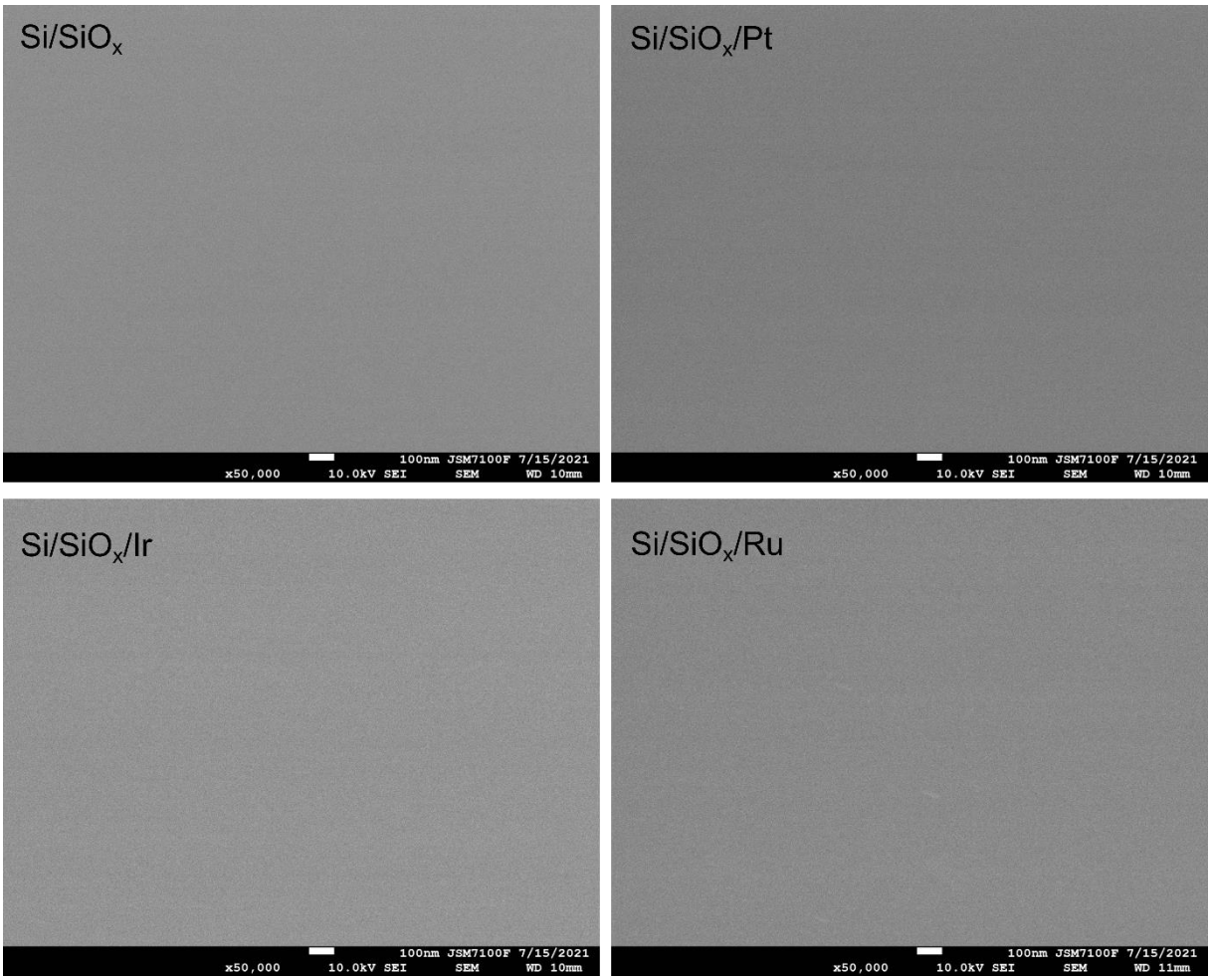

Figure S1. Top view SEM pictures showing the surface of p^{++}-Si/SiO_x, p^{++}-Si/SiO_x/Pt, p^{++}-Si/SiO_x/Ir, and p^{++}-Si/SiO_x/Ru. Scalebar = 100 nm.

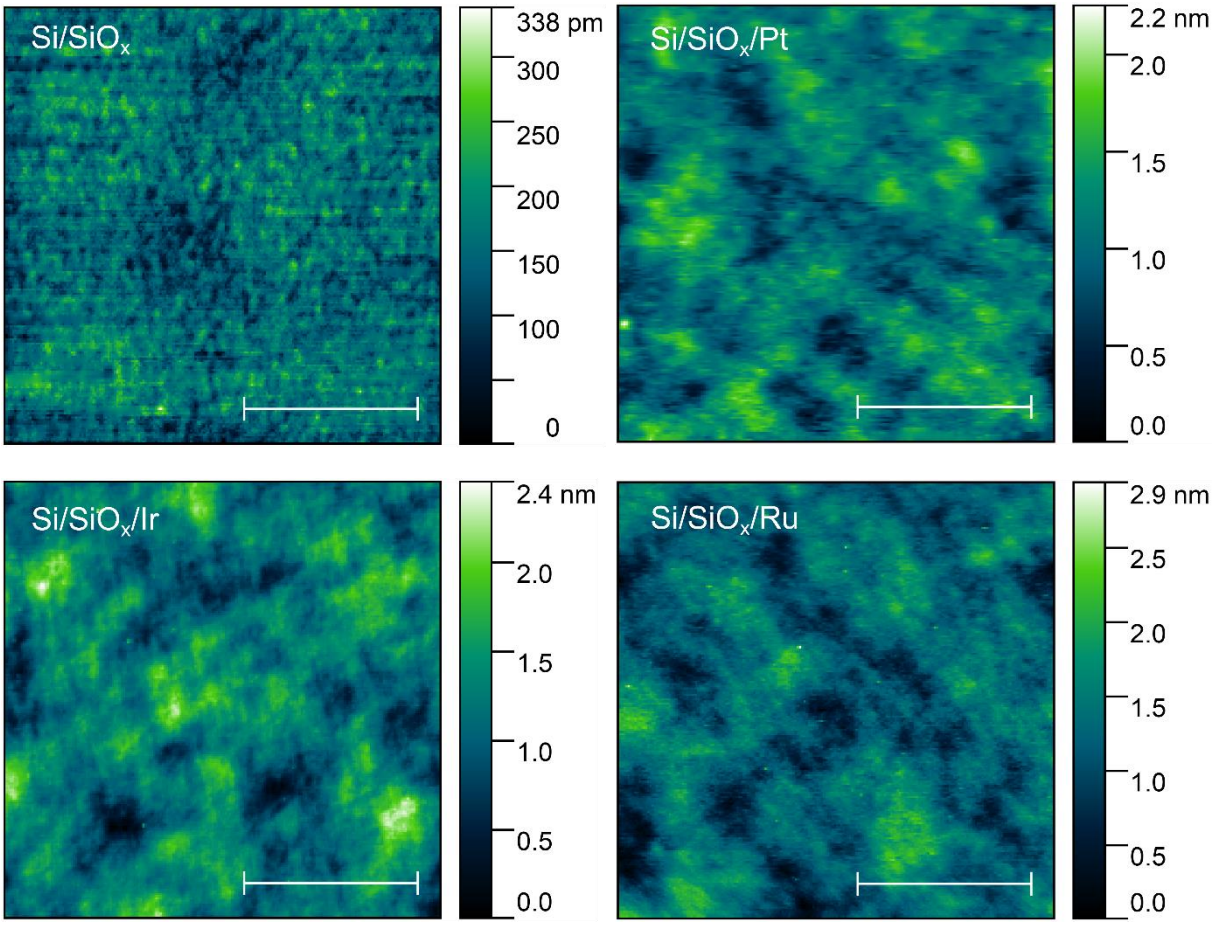

Figure S2. AFM pictures showing the surface of p^{++}-Si/SiO_x, p^{++}-Si/SiO_x/Ru, p^{++}-Si/SiO_x/Pt, and p^{++}-Si/SiO_x/Ir. Scalebar = 2 µm.

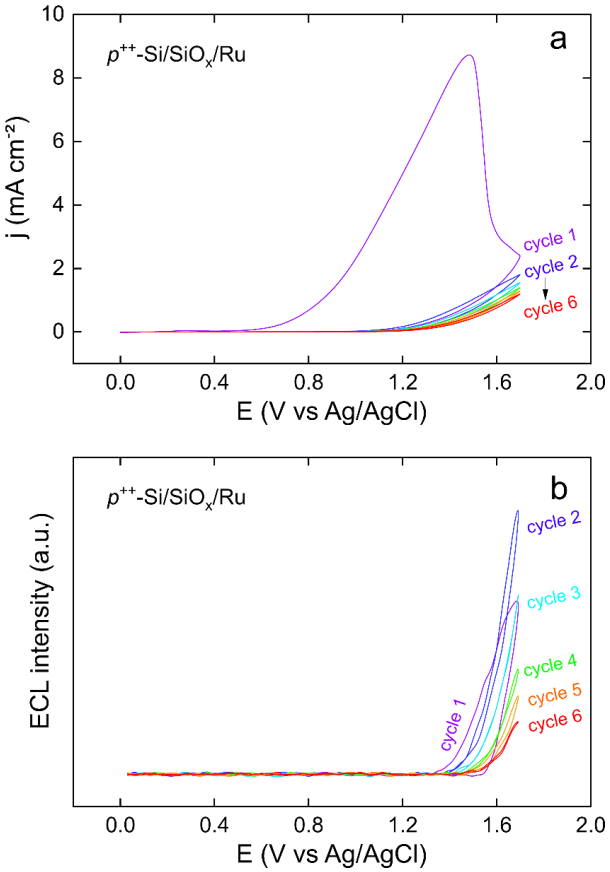

Figure S3. CVs measured in the dark (a) and corresponding ECL intensity profiles (b) in 100 mM TPrA and 5 mM $[Ru(bpy)_3]^{2+}$ in PBS on p^{++}-Si/SiO$_x$/Ru (50 mV s^{-1}).

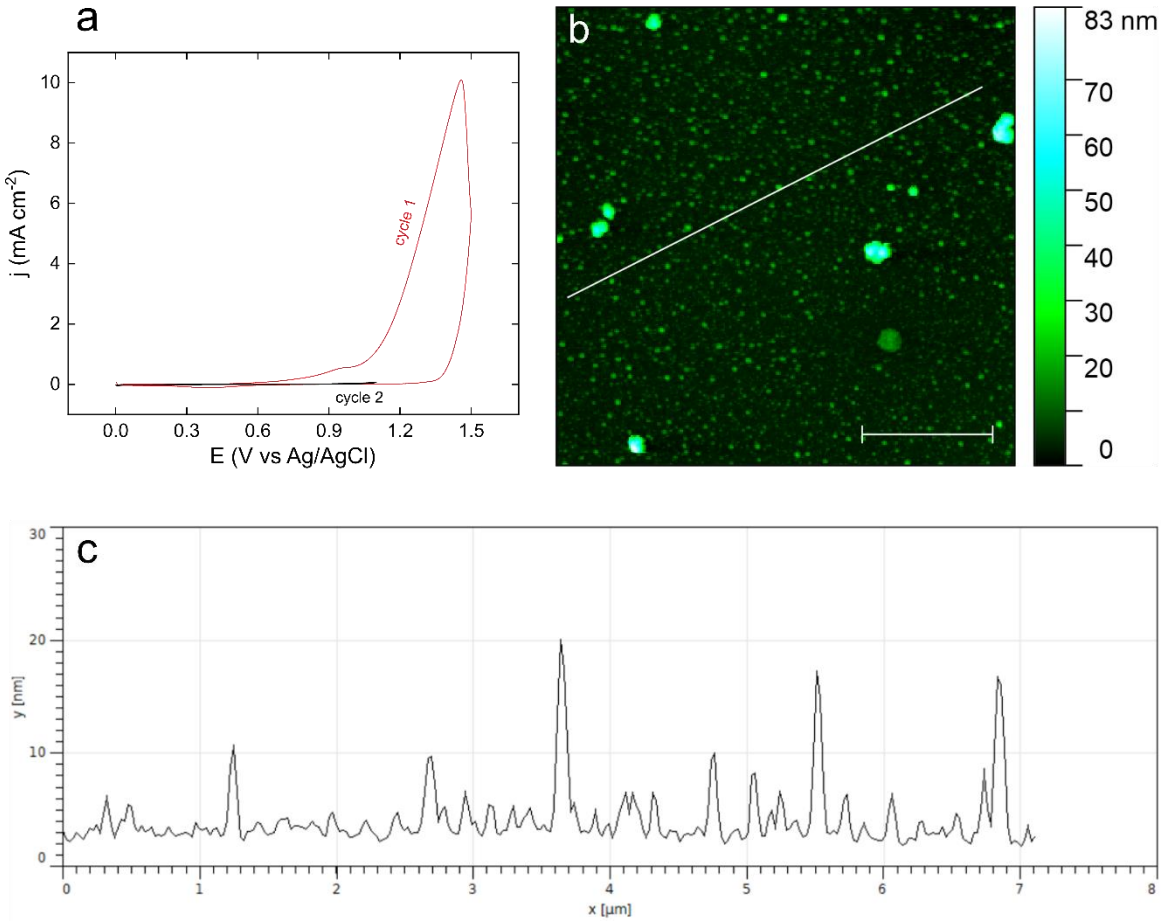

Figure S4. a) Two first CV cycles mesured in the dark in PBS on p^{++}-Si/SiO_x/Ru (50 mV s^{-1}). b) AFM picture of the surface of p^{++}-Si/SiO_x/Ru after electrochemical cycling (20 cycles) from 0 to 1.5 V in PBS with 100 mM TPrA and 5 mM $[Ru(bpy)_3]^{2+}$ at 50 mV s^{-1}. Scalebar = 2 µm. c) Height profile corresponding to the white line in the AFM picture.

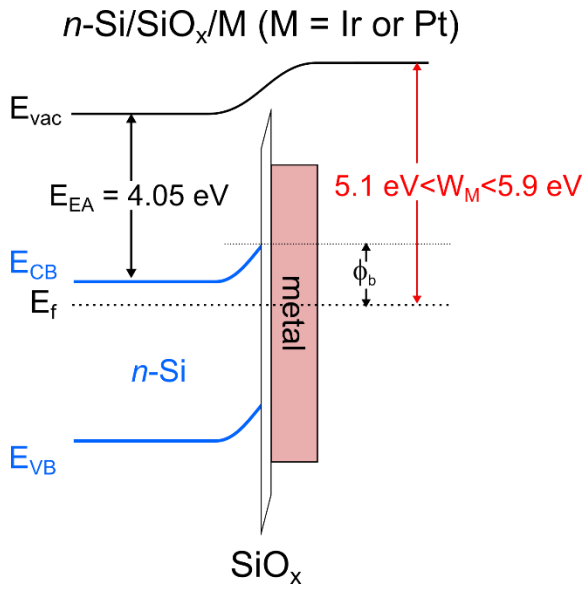

Figure S5. Schematic band diagram showing the barrier height (ϕ_b) at the *n*-Si/SiO_x/M junction. E_{EA} is the Si electron affinity, E_f is the Fermi level of Si, W_M is the work function of the metal.

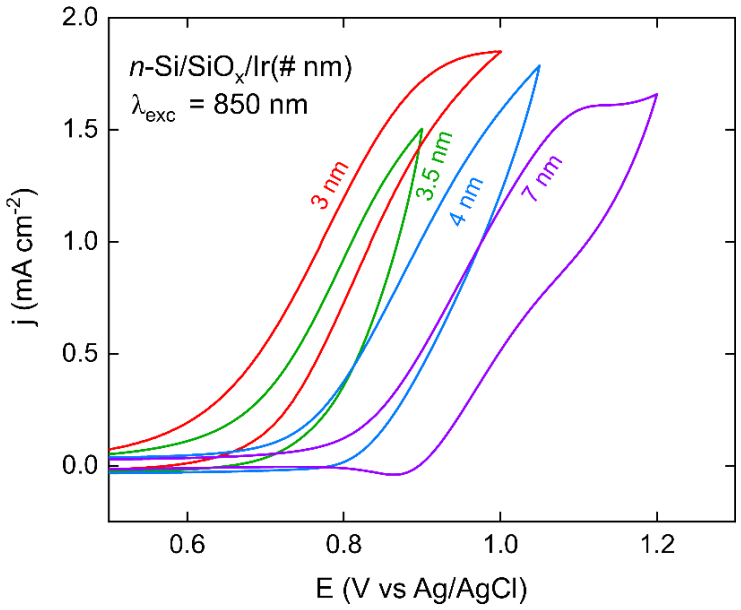

Figure S6. CVs measured at illuminated (λ_{exc} = 850 nm) *n*-Si/SiO_x/Ir photoanodes with Ir thin film having a thickness of 3 nm (red), 3.5 nm (green), 4 nm (blue), and 7 nm (purple) in PBS with 100 mM TPrA and 5 mM $[Ru(bpy)_3]^{2+}$ at 50 mV s^{-1}.

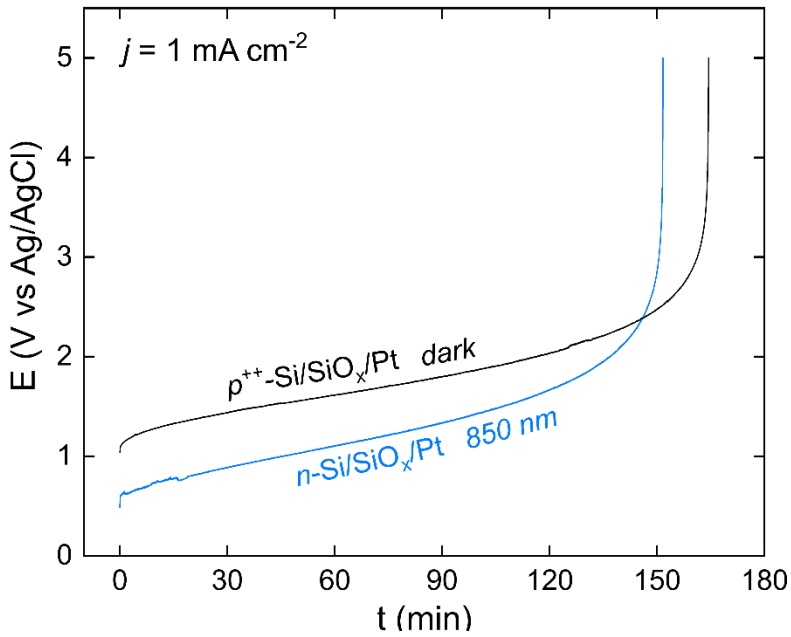

Figure S7. CP curves recorded in PBS with 100 mM TPrA and 5 mM $[Ru(bpy)_3]^{2+}$ at 1 mA cm^{-2} on p^{++}-Si/SiO_x/Pt (dark) in the dark and on *n*-Si/SiO_x/Pt (blue) under IR illumination (λ_{exc} = 850 nm).

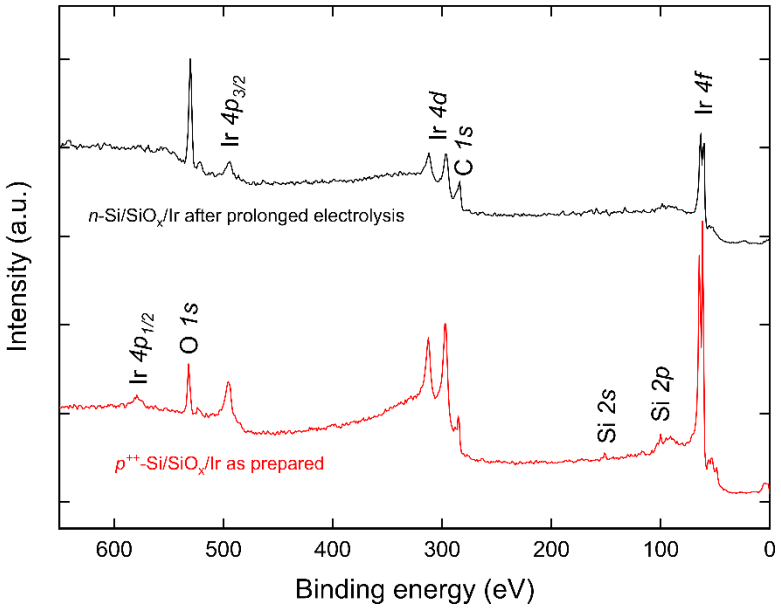

Figure S8. XPS spectra of the p^{++}-Si/SiO_x/Ir after preparation (red) and *n*-Si/SiO_x/Ir after a 33.5 h-long PECL test (black).

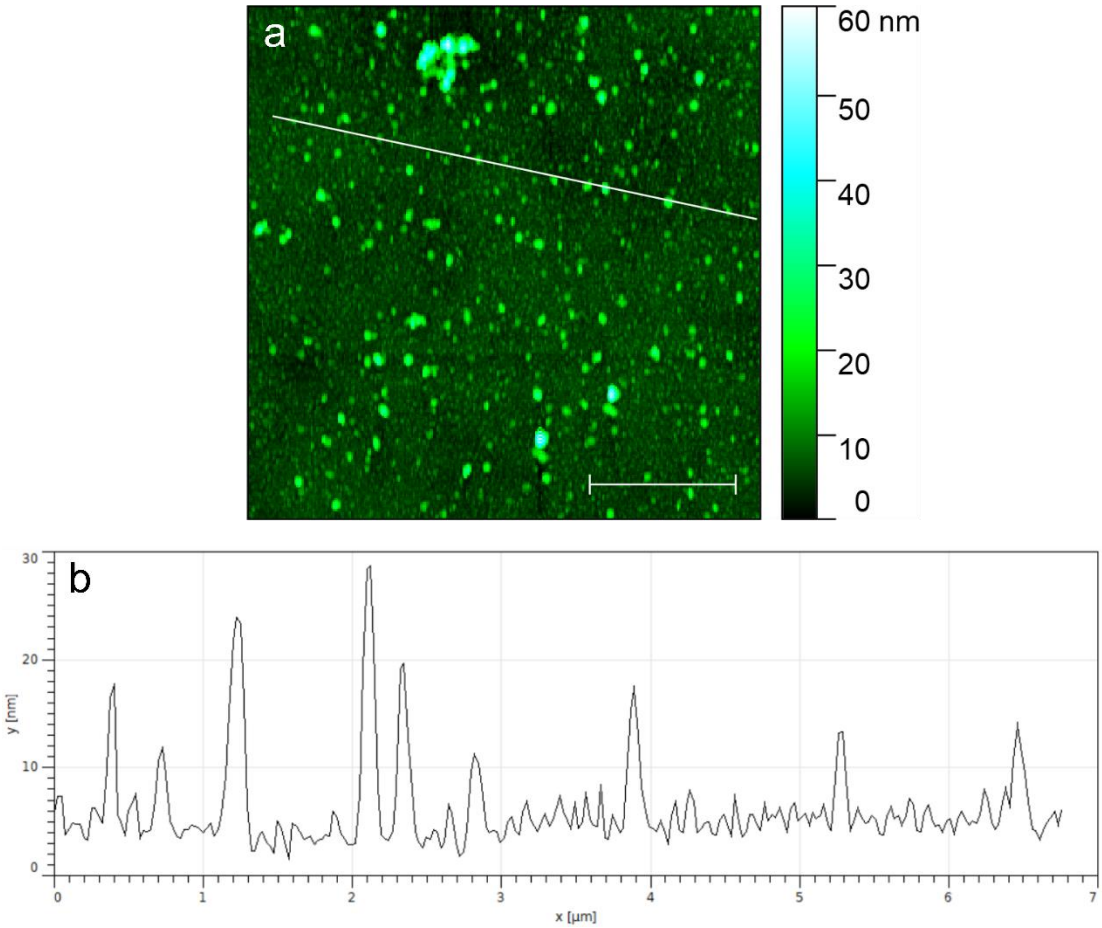

Figure S9. a) AFM picture of an *n*-Si/SiO_x/Ir surface after a prolonged PECL test of 33.5 h. Scalebar = 2 µm. b) Height profile corresponding to the white line in the AFM picture.

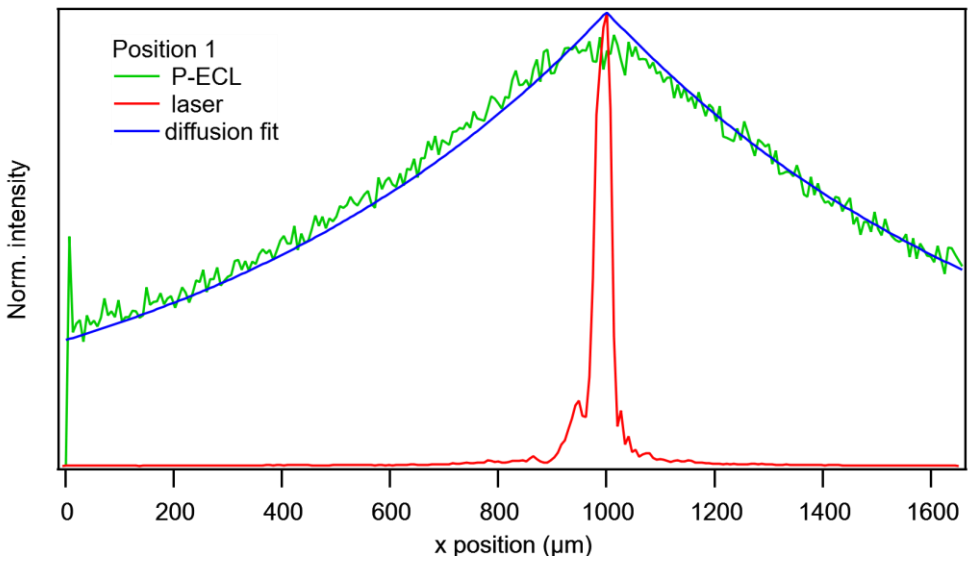

Figure S10. Exponential fit of the PECL spot profile. More information is given in Section 4 of the SI.

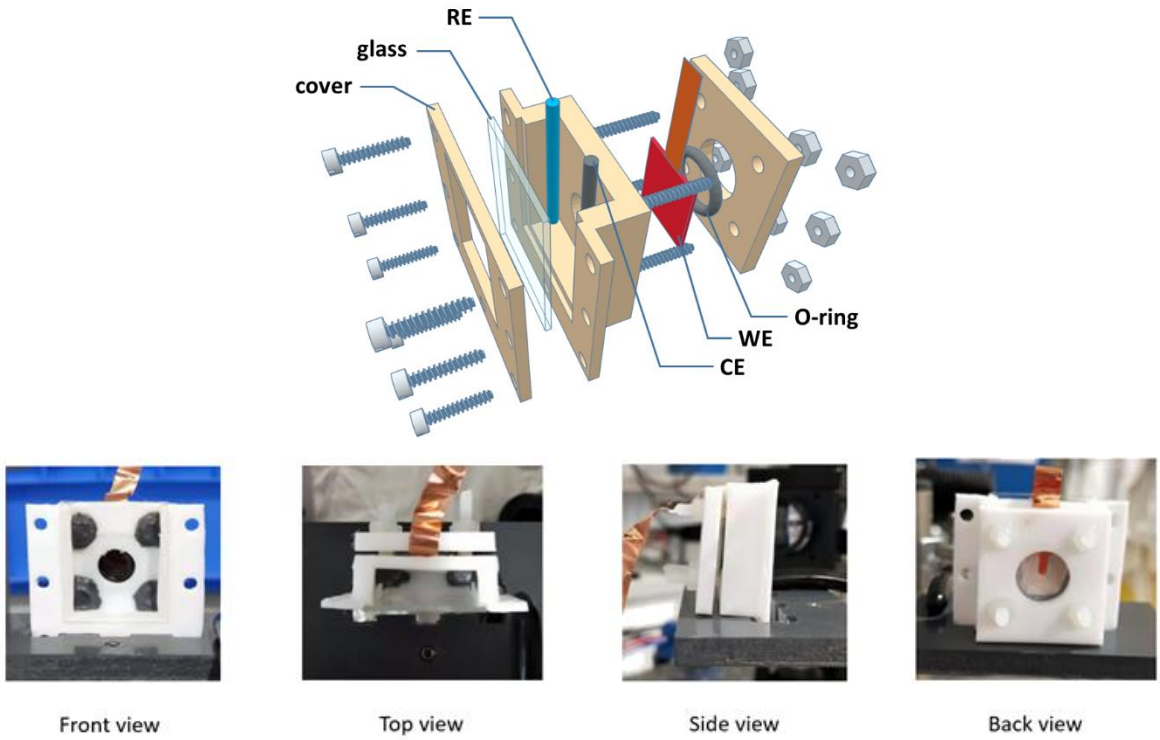

Figure S11. Scheme (top) and photographs (bottom) showing the PECL cell design.

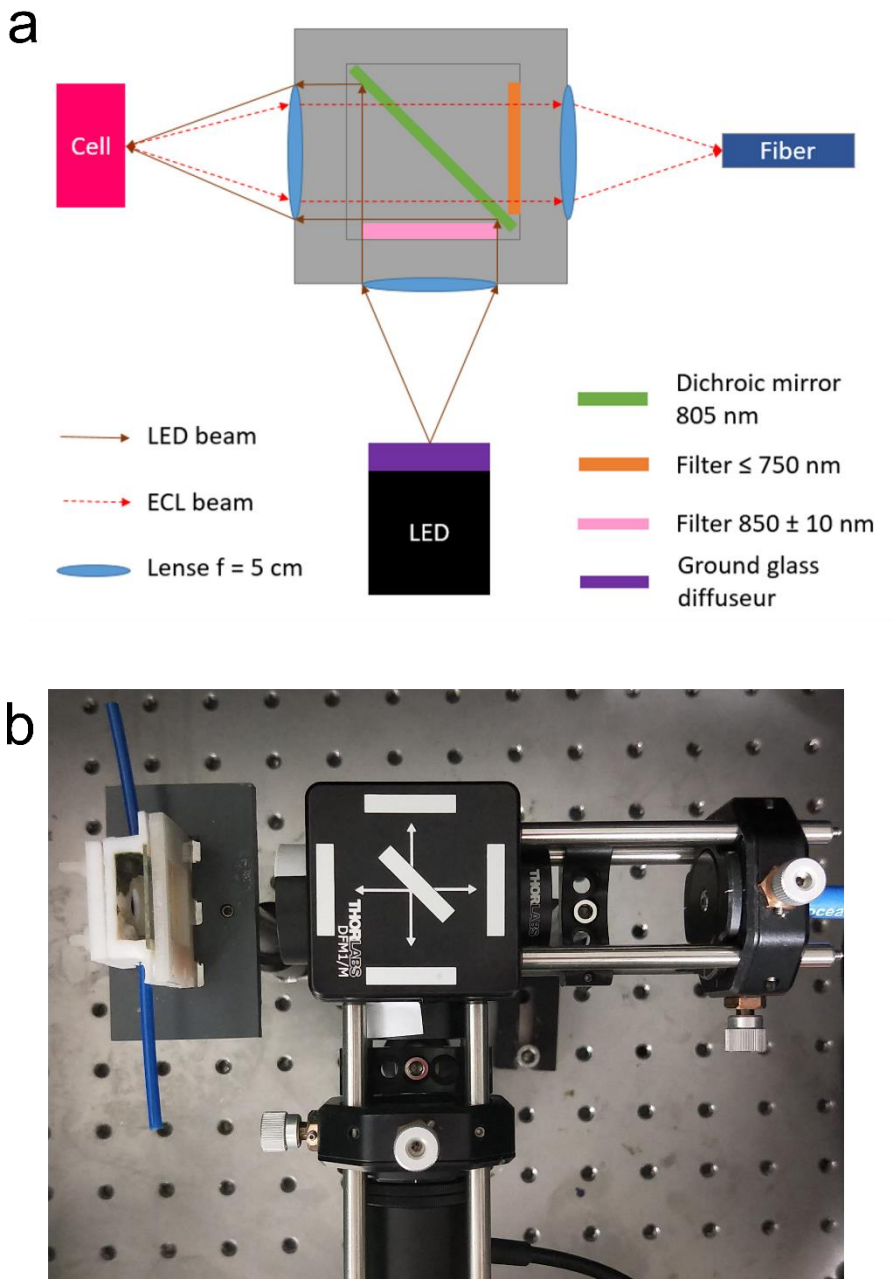

Figure S12. a) Scheme and b) photograph showing the PECL photoelectrochemical setup.

3. Supplementary table

Table S1. Characteristics of several reported PECL systems.

reference	PECL type	semiconductor	ECL system/process	electrolyte type	E_{app} (V)[a]	λ_{exc} (eV)	λ_{em} (eV)	λ shift (nm)	operation time (min)
1	**anti-Stokes**	*p*-Si *p*-InP *p*-GaAs	annihilation	organic	-[b]	1.7[c]	3	-316	≈2
2	**anti-Stokes**	*p,n*-GaAs *p,n*-InP	annihilation	organic	1.6[d]	<1.7	2.8[e]	-293	-[f]
3	**anti-Stokes**	*n*-Si	$[Ru(bpy)_3]^{2+}$ TPrA	aqueous	0.5	1.5	1.9	-175	15
4	**anti-Stokes**	*n*-Si	luminol	aqueous	-0.1	1.7[g]	2.9	-300	≈3
5	Stokes	*n*-$BiVO_4$	L-012[h]	aqueous	-0.4	3.3	2.5	128	120
6	Stokes	*n*-Fe_2O_3	L-012[h]	aqueous	-0.2	3.3	2.5	123	120
this work	**anti-Stokes**	*n*-Si	$[Ru(bpy)_3]^{2+}$ TPrA	aqueous	0.46	1.46	1.96	-218	2100

[a]: potential onset of the PECL emission, vs. Ag/AgCl, if not reported otherwise.
[b]: the reference electrode was not indicated.
[c]: λ_{exc} = 674 nm (1.8 eV) was also reported.
[d]: difference between the anodic E_{app} and cathodic E_{app} for *n*-GaAs.
[e]: for the TMPD/DPA system on *n*-GaAs.
[f] : no duration was reported.
[g]: λ_{exc} = 625 nm (2 eV) was also reported.
[h]: L-012 = 8-amino- 5-chloro-2,3-dihydro-7-phenyl-pyrido[3,4-d]pyridazine-1,4-dione.

4. Minority carriers diffusion length in crystalline *n*-Si and size of the PECL pattern

To understand the difference between the diameter of the IR laser beam, D_{beam} (30 µm) and that of the PECL spot, D_{PECL} (1.1 mm) in the site-selective PECL experiments presented in Figure 4, we first calculate the theoretical diffusion length (L_p) of the photogenerated holes in the phosphorous-doped Si substrate expected because of the doping level. The photoactive Si employed in this work has a resistivity ρ comprised between 0.3 – 0.7 Ω cm, as given by the manufacturer. Consequently, we consider here a resistivity of 0.5 Ω cm, which, corresponds, at T = 300 K, to a dopant concentration of N_D = 1 x10^{16} cm^{-3}, a minority carrier diffusivity D_p = 11.24 cm^2 s^{-1}, and a minority carrier mobility of μ_p = 434.8 cm^2 V^{-1} s^{-1} for this type of Si according to the free online resource for photovoltaic PV Lighthouse, accessible at the following link.[7]

The hole lifetime, τ_p, for *n*-type Si with N_D = 1 x10^{16} cm^{-3} can be estimated as 0.1 ms according to the literature.[8–10] Then, the hole diffusion length (L_p) can be calculated using the following equation:

$$L_p = \sqrt{D_p \times \tau_p} \qquad (1)$$

Using the previously determined value of D_p = 11.24 cm^2 s^{-1} and τ_p = 1 x10^{-4} s, a value of L_p = 335 µm is found.

As shown in Figure S10, the ECL spot profile can be fitted with a simple exponential decay suggesting that the minority carrier diffusion regime is valid. However, the fitted diffusion length of 800 µm is larger than the theoretical one obtained above. In the present experiment, we observe a lateral diffusion which occurs within an electron depletion layer in the semiconductor, where the hole lifetime should locally increase significantly. This can explain the larger value of the hole diffusion length observed in our experiment.

According to this calculation, we can quite confidently estimate that the good diffusion of holes in Si is the main cause for low resolution, as pointed out by other reports.[11] In addition, other factors may lead to a further increase in the spot size. First, the presence of the metal thin film may promote a longer diffusion length of the carrier at the interface by increasing in-plane lateral conductivity. Second, the rather slow kinetic of the ECL reaction probably leads to an increase of the PECL size as all the photogenerated holes cannot be consumed rapidly at the location where they are generated, as previously described.[12] Finally, the convection condition that was used to avoid deleterious mass transport limitation, may also lead to the increase of the PECL pattern because, in this case, the oxidized species may react further away from their generation location.[13] The latter hypothesis is, however, less probable because the flow was directed laterally in the cell and the PECL patterns always had a disk shape.

5. References

1 D. Laser and A. J. Bard, *Chem. Phys. Lett.*, 1975, **34**, 605–610.

2 J. D. Luttmer and A. J. Bard, *J. Electrochem. Soc.*, 1979, **126**, 414–419.

3 Y. Zhao, J. Yu, G. Xu, N. Sojic and G. Loget, *J. Am. Chem. Soc.*, 2019, **141**, 13013–13016.

4 Y. B. Vogel, N. Darwish and S. Ciampi, *Cell Rep. Phys. Sci.*, 2020, **1**, 100107.

5 J. Yu, H. Saada, R. Abdallah, G. Loget and N. Sojic, *Angew. Chemie Int. Ed.*, 2020, **59**, 15157–15160.

6 J. Yu, H. Saada, N. Sojic and G. Loget, *Electrochim. Acta*, 2021, **381**, 138238.

7 K. McIntosh, M. Abbott and B. Sudbury, PV lighthouse, https://www.pvlighthouse.com.au, (accessed 22 December 2021).

8 M. E. Law, E. Solley, M. Liang and D. E. Burk, *IEEE Electron Device Lett.*, 1991, **12**, 401–403.

9 J. A. del Alamo and R. M. Swanson, *Solid. State. Electron.*, 1987, **30**, 1127–1136.

10 IOFFE semiconductor database, http://www.ioffe.ru/SVA/NSM/Semicond/, (accessed 22 December 2021).

11 Y. B. Vogel, J. J. Gooding and S. Ciampi, *Chem. Soc. Rev.*, 2019, **48**, 3723–3739.

12 H. Zhu, B. Miller and D. Scherson, *J. Electrochem. Soc.*, 2010, **157**, F137.

13 L. L. Shultz, J. S. Stoyanoff and T. A. Nieman, *Anal. Chem.*, 1996, **68**, 349–354.